Photoproduction total cross section and shower development

F. Cornet,[1] C. A. García Canal,[2] A. Grau,[1] G. Pancheri,[3] and S. J. Sciutto[2]

[1]*Departamento de Física Teórica y del Cosmos and Centro Andaluz de Física de Partículas, Universidad de Granada, E-18071 Granada, Spain.*

[2]*Departamento de Física, Universidad Nacional de La Plata, IFLP, CONICET, C. C. 67, 1900 La Plata, Argentina.*

[3]*INFN Frascati National Laboratories, Via Enrico Fermi 40, I-00044 Frascati, Italy.*

The total photoproduction cross section at ultra-high energies is obtained using a model based on QCD minijets and soft-gluon resummation and the ansatz that infrared gluons limit the rise of total cross sections. This cross section is introduced into the Monte Carlo system AIRES to simulate extended air-showers initiated by cosmic ray photons. The impact of the new photoproduction cross section on common shower observables, especially those related to muon production, is compared with previous results.

I. INTRODUCTION

The determination of the composition of ultra-high energy (UHE), i.e. with energies lager than $10^{18}\ eV$, cosmic rays is an important open problem in cosmic ray physics. A good knowledge of the percentage of protons, heavy nuclei and photons hitting the atmosphere can provide important clues to understand the origin of those cosmic rays and their acceleration mechanism. The Pierre Auger Observatory [1] has devoted big efforts to this end and they have recently determined that the composition of UHE cosmic rays varies from mainly protons at $E = 10^{17.5}\ eV$ to have an important presence of heavy nuclei at $E = 10^{19.5}\ eV$ [2]. However, as no photons have been found up to now, the following bounds on the fraction of photons arriving to Earth have been set: 3.8%, 2.4%, 3.5% and 11.7% for photon energies above $2\times10^{18}\ eV$, $3\times10^{18}\ eV$, $5\times10^{18}\ eV$ and $10\times10^{18}\ eV$, respectively [3]. An important parameter to obtain these bounds is the photon-proton total cross section from which one can estimate the photon-nucleus total cross section.

There are no experimental values for $\sigma^{\gamma p}_{total}$ at the very high cosmic ray energies, so one has to rely on extrapolations of accelerator data that in the case of photoproduction are limited to $\sqrt{s} \lesssim 200\ GeV$. Consequently the extrapolation to higher energies leaves considerable uncertainties. A possibility is to use recent LHC data, right now up to $\sqrt{s} = 8\ TeV$, and use models describing both photoproduction and $proton - proton$ scattering to infer, from pp data, the higher energy behavior of $\sigma^{\gamma p}_{total}$. Notice that the release of LHC data on the total proton-proton cross section, has led most current hadronic models to slight adjustments of the model parameters. The reason follows from the fact that lower energy data on hadron-hadron scattering, notably at $\sqrt{s} = 540\ GeV$ and $1800\ GeV$ had an uncertainty of 10% or more. Thus, often, a band, rather than a single curve, was provided. After TOTEM data appeared [4, 5], the models could be sharpened taking into account the much smaller error reported. On its turn, this sharpened tuning could be used for the high energy extrapolation of $\sigma^{\gamma p}_{total}$.

Here we shall follow the mentioned procedure. The updating of previous predictions [6] for $\sigma^{\gamma p}_{total}$ on the basis of LHC data, are then used as input to the AIRES [7] system to simulate extended air showers initiated by photons.

The model for the total cross section,which we apply here, includes basic QCD inputs such as the parton densities obtained from experiments and well known QCD subprocess

cross sections [8]. A few non-perturbative parameters are also included. These ingredients allowed the search for the effects of the hadronic structure of the photon through the analysis of the total cross sections in which they are involved.

In summary, the model developed in [8] is based upon the use of:

- QCD mini-jets to drive the rise of the total cross section in the asymptotic regime;
- The eikonal representation for the total cross section using a purely imaginary *overlap function*, obtained from mini-jet QCD cross sections;
- The impact parameter distribution, input for the eikonal, obtained from the Fourier transform of the re-summed soft gluon transverse momentum distribution;
- The resummation of soft gluon emission down to zero momentum.

The last element is the specific feature of this model, hereafter called BN-model from the well known Bloch and Nordsieck [9] study of the infrared catastrophe, which occurs in electrodynamics when the soft photon momentum goes to zero. In the model, the re-summation of QCD soft gluons is applied, and covers the region where $k_t^{gluon} \to 0$ with an ansatz, discussed below. One should notice that the main difference of this proposal with respect to other mini-jet models comes from the energy dependence of the impact parameter distribution and from soft gluon k_t-resummation extended to zero momentum modes. The model to be presented in the next section probes into this region.

II. THE BLOCH-NORDSIECK (BN) MODEL FOR TOTAL CROSS SECTIONS

In this section we shall update previous results from the BN model for the $\gamma - p$ total cross section [6], which will be input to the AIRES simulation program.

The BN model [8] is based on two features of all hadronic cross sections:

- As the c.m. energy increases from fixed target experiments to those at colliders, both purely hadronic and with photons, such as HERA (γp), all total cross sections first decrease and then, around $\sqrt{s} = 10 - 20\ GeV$ for the pp case, start increasing. Mini-jet models attribute this transition to the onset of hard and semi-hard parton-parton collisions, which can be described by perturbative QCD. Such a suggestion

was advanced long time ago [10] when proton-proton scattering at the CERN ISR [11] confirmed the rise which cosmic ray experiments had already seen [12]. The large errors affecting the cosmic ray experimental data had cast uncertainty on a definite conclusion, but the ISR measurements definitively confirmed the rise, which was soon interpreted as a clear indication of the composite parton picture we are familiar with today. The role of mini-jets both in minimum bias physics [13] and in the rise of the total cross section [14] was then further developed and is input to many simulation programs.

- The observed rise, which may initially be considered to follow a power law, must obey the limitations of the Froissart bound, namely

$$\sigma_{total}(s) \simeq [\ln s]^2 \quad as \quad s \uparrow \quad at \quad most \tag{1}$$

where the bound is connected to the existence of a cut-off in impact parameter space [15].

Both features are embedded into figure 1, where the proton and photon cross sections are shown together, normalized at low energy, to highlight their common features. The yellow band, superimposed to the data, comes from the BN model we shall describe below.

The first feature of the total cross section, i.e. the rise at high energy, is obtained in mini-jet models, through a perturbative calculation based on the QCD jet cross section, namely

$$\sigma_{\rm jet}^{AB}(s, p_{tmin}) = \int_{p_{tmin}}^{\sqrt{s}/2} dp_t \int_{4p_t^2/s}^{1} dx_1 \int_{4p_t^2/(x_1 s)}^{1} dx_2 \times \sum_{i,j,k,l} f_{i|A}(x_1, p_t^2) f_{j|B}(x_2, p_t^2) \frac{d\hat{\sigma}_{ij}^{kl}(\hat{s})}{dp_t}, \tag{2}$$

with $A, B = p, \bar{p}, \gamma$, and $d\hat{\sigma}_{ij}^{kl}(\hat{s})/dp_t$ is the parton-parton differential cross section, calculable from QCD, with the running coupling constant of asymptotic freedom expression. The parameter $p_{tmin} \approx 1 - 2$ GeV separates hard processes, for which one can use a perturbative QCD description, from the soft ones which dominate at low c.m. energy of the scattering hadrons. The mini-jet cross section gets its name because is dominated by low-p_t processes, which cannot be identified by jet finding algorithms, but can still be perturbatively calculated using parton-parton sub-processes and DGLAP evoluted LO Partonic Density Functions (PDFs) $f_{i|A}$, such as GRV [16], MRST [17], CTEQ [18] for the proton or GRV[19], GRS [20] and CJKL [21] for the photon.

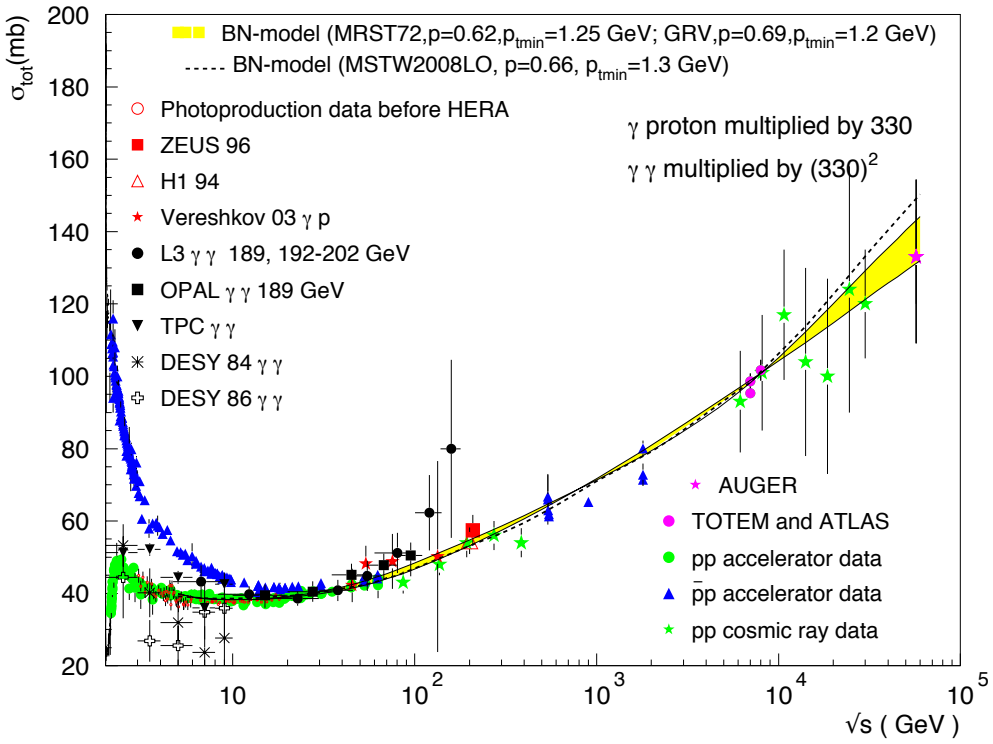

FIG. 1. Total proton-proton, $p\bar{p}, \gamma p, \gamma\gamma$ cross sections, normalized at low energy so as to show common features. This figure is updated from [6] to include recent data. The yellow band and the dashed line are obtained from a description of pp scattering with an eikonal model inclusive of mini-jets and soft gluon resummation, described in the text and called BN model.

The expression of equation (2) gives a mini-jet cross section which rises very fast with energy. In order to ensure unitarity [14], the mini jet cross section is embedded in an eikonal representation, whose implementation requires modeling the impact parameter space of the colliding hadrons. We notice that, in order to obey the limitations imposed by the Froissart bound [15], such modeling should include a large distance cut-off. In the BN model this is obtained by means of soft gluon resummation down to zero momentum gluons.

In eikonal mini-jet models one starts with

$$\sigma_{tot} = 2 \int d^2\mathbf{b} \left[1 - e^{-n(b,s)/2}\right] \tag{3}$$

where b is the impact parameter and the real part of the eikonal has been neglected. This is a good approximation at high energy. The average number of collisions $n(b,s)$ can be

split into a soft contribution which will be parameterized with a suitable non-perturbative expression, and a perturbative (pQCD) term where both hard and soft gluon emission contribute, namely $n(b,s) = n_{soft}(b,s) + n_{hard}(b,s)$. In the mini-jet model of [8] the authors propose

$$n_{hard}(b,s) = A_{BN}(b,s)\sigma_{jet}(s) \tag{4}$$

with

$$A_{BN}(b,s) = N \int d^2\mathbf{K}_\perp \; e^{-i\mathbf{K}_\perp\cdot\mathbf{b}} \frac{d^2P(\mathbf{K}_\perp)}{d^2\mathbf{K}_\perp} = \frac{e^{-h(b,q_{max})}}{\int d^2\mathbf{b} \; e^{-h(b,q_{max})}} \tag{5}$$

and

$$h(b,q_{max}) = \frac{16}{3}\int_0^{q_{max}} \frac{\alpha_s(k_t^2)}{\pi}\frac{dk_t}{k_t}\log\frac{2q_{\max}}{k_t}[1 - J_0(k_t b)] \tag{6}$$

The physical content of equation (5) is as follows: $A_{BN}(b,s)$ is obtained as the Fourier transform of the probability $d^2P(\mathbf{K}_\perp)/d^2\mathbf{K}_\perp$ that, in a collision between two collinear partons, soft gluon emission gives rise to an overall transverse momentum unbalance $\mathbf{K}_\perp$. This probability can be calculated through resummation of all soft gluons emitted in an otherwise collinear parton-parton collision. This leads to the exponentiation of the integrated single soft gluon spectrum, given by the function $h(b,q_{max})$ of equation (6).

The energy parameter q_{max} represents the maximum transverse momentum for *single* gluon emission and embeds the kinematics of the process

$$parton_1 + parton_2 \rightarrow jet_1 + jet_2 + initial\ state\ emitted\ gluon \tag{7}$$

Its calculation is detailed in [22] and follows the original formulation of [23]. As shown in [22], the energy parameter q_{max} depends linearly on the p_t of the final state partons which, at leading order, are described as hadronizing in two jets. This is a description, which should hold at LO and upon averaging over all densities and sub-processes. Thus q_{max} depends on the PDFs chosen for the calculation of the mini jet cross section. A description of q_{max} and its dependence upon energy, PDFs and p_{tmin} was recently presented in [24] for purely proton processes for the photon case, it can be found in [6].

Because the acollinearity introduced by soft gluon emission reduces the cross section, the distribution of equation (5) can give a cut-off in **b**-space, dynamically generated by soft gluon emission and thus can reduce the very fast rise due to the mini-jet cross section. This effect is energy dependent, and increasing through the energy parameter q_{max}, with the strength of the cut-off depending on the infrared region. This region is crucial to the calculation of the very large impact parameter processes, dominating all total cross sections.

In the BN model, the zero momentum gluon contribution is implemented by means of a singular but integrable behavior of the quark-gluon coupling constant in the infrared region, characterized by a singularity parameter $1/2 < p < 1$. For details we refer the reader to references [8, 25]. To fit this parameter, in this model one uses the expression

$$\alpha_s(k_t^2) = \frac{12\pi}{33-2N_f}\frac{p}{\ln[1+p(\frac{k_t}{\Lambda_{QCD}})^{2p}]} \xrightarrow{k_t\to 0} \frac{12\pi}{33-2N_f}(\frac{\Lambda_{QCD}}{k_t})^{2p}. \tag{8}$$

This expression reduces to the usual asymptotic freedom expression for $k_t >> \Lambda_{QCD}$, while the singular behavior for $k_t \to 0$ leads to a cut-off in impact parameter space, which is exponential for $p = 1/2$, almost gaussian for $p \lesssim 1$, and provides a mechanism for the implementation of the Froissart bound. As it was shown in [25], the singular behavior of the coupling constant in the infrared limit leads to a large impact parameter behavior such as $A_{BN}(b,s) \simeq exp[-(b\bar{\Lambda})^{2p}]$. When coupled with the strong rise of the mini jet cross section $\sigma_{jet} \simeq s^{\epsilon}$, with $\epsilon \simeq 0.3-0.4$, one obtains

$$\sigma_{total}^{pp} \to [\ln s]^{1/p} \qquad \sqrt{s} \to \infty \tag{9}$$

The singularity parameter p together with p_{tmin} and the choice of PDFs determine completely $n_{hard}(b,s)$ and constitute the *high energy parameter set* of the BN model. The choice of LO rather than next-to-leading order densities is discussed in [8] and follows from the ansatz that resummation takes into account most of the major next-to-leading order contributions. The remaining uncertainty, from non-resummed finite radiative corrections, is included in the parameters p and p_{tmin}, which are determined phenomenologically.

Prior to the start of LHC, with the above inputs, and a phenomenological parameterization of the low energy region, the BN model gave a good description of pp and $p\bar{p}$ total cross sections, predicting $\sigma(\sqrt{s} = 14\ TeV) = 100 \pm 12\ mb$ [26]. The error corresponds to different choices of the PDFs and of the parameter set $\{p, p_{tmin}\}$ and reflects the difficulty of determining the optimal sets of parameters, because of the large error from $p\bar{p}$ measurements at $Sp\bar{p}S$ and TeVatron energies.

The measurement of the total pp cross section at LHC at energies $\sqrt{s} = 7$ and $8\ TeV$ has allowed to reduce the parametric uncertainties present in most models. In figure 1 we present our updated analysis, with a band corresponding to the predictions for pp obtained with two different sets of LO PDFs, MRST and GRV. The yellow band shows how the BN model accommodates recent results for σ_{total}^{pp}, including the extraction of the pp cross

sections from cosmic ray measurement by the AUGER collaboration, at $\sqrt{s} = 57\ TeV$ [27]. With the choice of parameters as indicated in the figure and the set of MRST densities from [17], the value expected at $\sqrt{s} = 14\ TeV$ is $\sigma^{pp}_{total} = 112.24\ mb$. In addition, we also plot pp results obtained in [24] using more recent PDFs, such as MSTW08, indicated by the dashed line. Using older LO densities, such as GRV [16], one can also obtain a good description i.e. $\sigma^{pp}_{total} = 109.3\ mb$, namely, once the TOTEM, ATLAS and AUGER points (with their errors) are included in the description, the results, for different densities, are rather stable up to LHC energies. However, it must be pointed out that beyond the present LHC range ($\sqrt{s} = 7,\ 8\ TeV$), there is a band of uncertainty in the model predictions, which corresponds to different extrapolations of the low x behavior of the densities as the energy increases. When the next LHC data will be available, this band will hopefully be narrowed further. In the meanwhile, in the update of our γp results to be described next, we shall use for the proton the same two sets of LO PDFs, MRST and GRV, used by our code in [6]. This choice may be modified in future applications.

We can now update the model for γp, which had been proposed before the LHC. In [6], following the model proposed by Fletcher, Gaisser and Halzen in [28], the BN model had been applied to photoproduction with the following minimal modifications :

$$\sigma^{\gamma p}_{tot} = 2P_{had} \int d^2b \left[1 - e^{-n^{\gamma p}(b,s)/2}\right] \tag{10}$$

$$P_{had} = \sum_{V=\rho,\omega,\phi} \frac{4\pi\alpha}{f_V^2} \tag{11}$$

$$n^{\gamma p}(b,s) = n^{\gamma p}_{soft}(b,s) + n^{\gamma p}_{hard}(b,s)$$

$$= n^{\gamma p}_{soft}(b,s) + A(b,s)\sigma^{\gamma p}_{jet}(s)/P_{had} \tag{12}$$

$$n^{\gamma p}_{soft}(b,s) = \frac{2}{3} n^{pp}_{soft}(b,s) \tag{13}$$

The extension to photon process requires the probability P_{had} that the photon behaves like a hadron [28, 29]. This quantity is non perturbative and could have some mild energy dependence. However, to minimize the parameters, it was taken to be a constant, estimating it through Vector Meson Dominance. In the analysis of [6], the value $P_{had} = \frac{1}{240}$ was used.

To determine the γp cross section that will be used as input to the AIRES shower simulation program [7], we use equation (10). We update the values of the model parameters to take into account the impact of the recent LHC [4, 5, 30] and AUGER Observatory [27] results on the pp cross section, which have appeared after the original analysis of [6].

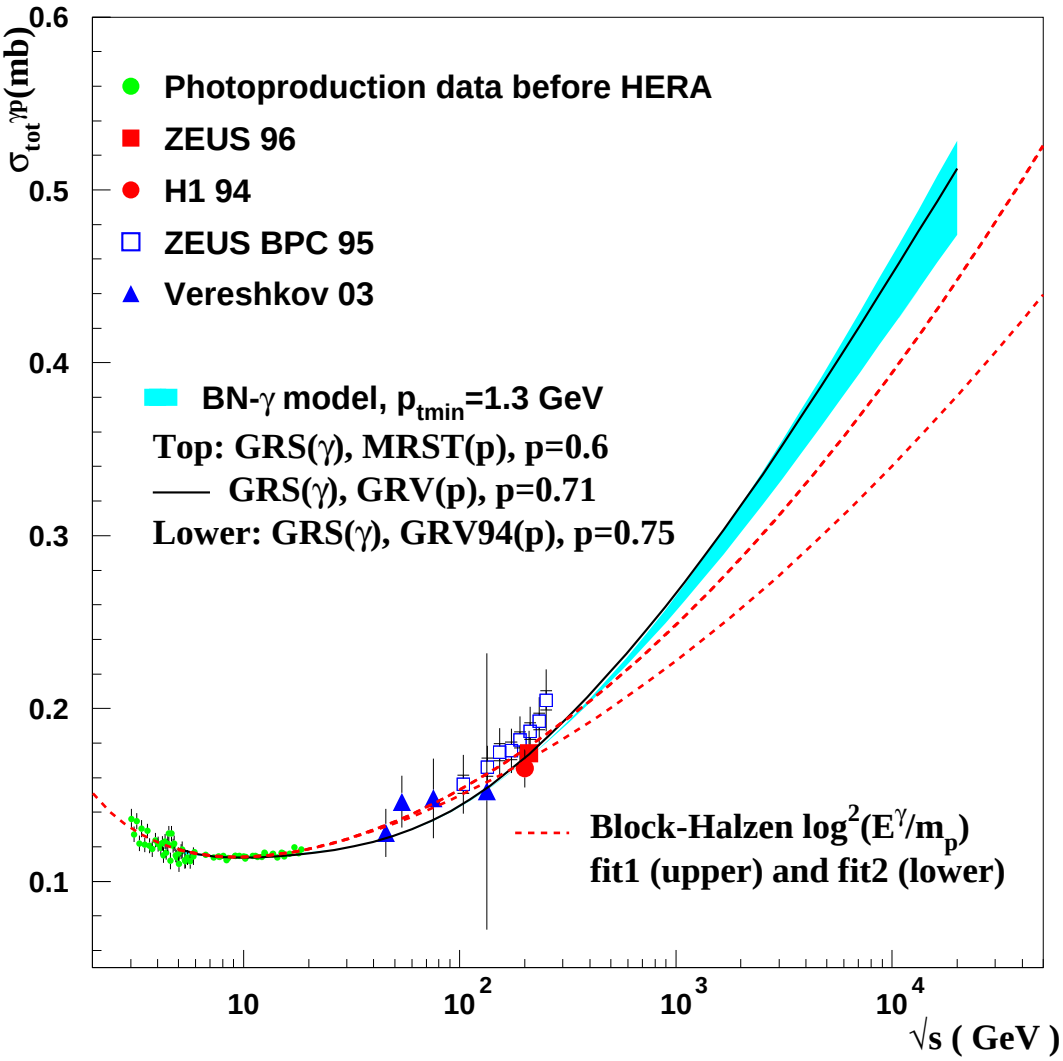

FIG. 2. Total photoproduction cross section and its description with the BN model, and with the analytic model of ref. [31, 32].

The result is shown in figure 2, with a band of values for $\sigma_{total}^{\gamma p}$ and it is compared with fits by Block and collaborators [31, 32], which impose a Froissart-limit saturating the high energy behavior. The band reflects results from the BN model with two different PDF sets. For this application of the BN model, labeled as $BN-\gamma$, we have used GRS densities for the photon, and the two PDF sets for the proton as in figure 1. The most recent type of PDFs, MSTW2008 [33], gives results similar to MRST for pp, and have similar uncertainties in the extrapolation to higher, AUGER type, energies [24]. Other parameters are obtained by comparison with the proton-proton results, within a few percent from those which give

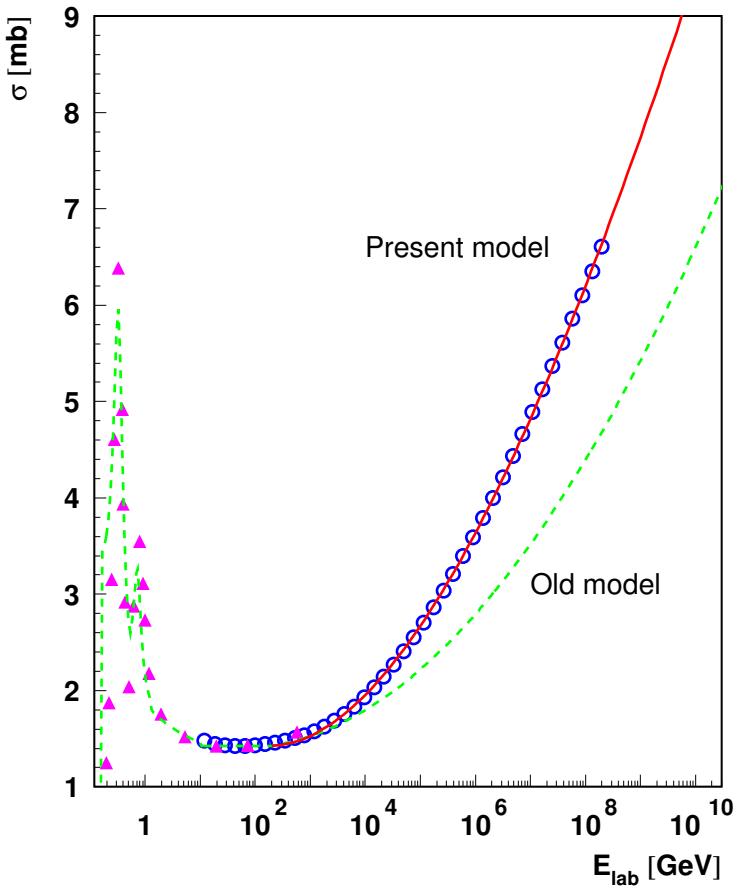

FIG. 3. Photon-air nucleus cross sections used in our simulations, plotted versus the photon lab energy. The triangles correspond to experimental data taken from reference [35]. The open circles correspond to the present model, and the solid line corresponds to a fit to these data, valid for energies greater than 200 GeV. The dashed line corresponds to the cross sections used in AIRES.

the yellow band for proton-proton in figure 1.

III. SIMULATION RESULTS

We have performed simulations of extended air showers using the AIRES system [7] linked to the package QGSJET-II [34] for processing high energy hadronic interactions. We have run two sets of simulations, namely, (1) using the cross sections for photonuclear reactions at energies greater than 200 GeV that are provided with the currently public version of AIRES; and (2) replacing those cross sections by the ones corresponding to the present model. More precisely, we have chosen to use the γp cross sections corresponding to the

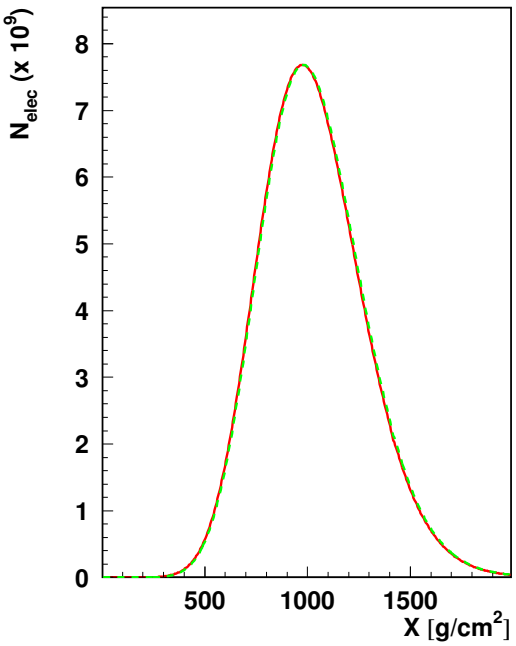

FIG. 4. Longitudinal development of electrons and positrons for 10^{19} eV photon showers inclined 60 degrees; ground at sea level. The solid (dashed) line corresponds to simulations with the present (old) model for the photonuclear cross section.

upper curve of the blue band in figure 2 and fit 2 of [31, 32], appropriately scaled to give the photon-air cross section required in AIRES. We are going to refer to sets (1) and (2) as "old model" and "present model", respectively. In figure 3 the gamma-air nucleus cross sections corresponding to both sets are displayed as a function of the photon lab energy. The triangles correspond to experimental data taken from reference [35], while the open circles correspond to numerical calculations using the present model, and is valid for energies greater than 200 GeV. The dashed line corresponds to the up to now standard cross sections implemented in AIRES, the "old model" [31]. Notice that for energies below 200 GeV we always use the same cross sections, which are calculated from fits to experimental data.

An important case to study the impact of changing the photonuclear cross sections at high energy is the case of showers initiated by photons. In such showers, the photonuclear reactions constitute the main channel for hadron production, which in turn are responsible for the production of muons, mainly via pion decay. It is a well known fact that showers initiated by photons have noticeably less muons than showers initiated by hadrons, and this is one of the features used to discriminate photonic from hadronic showers.

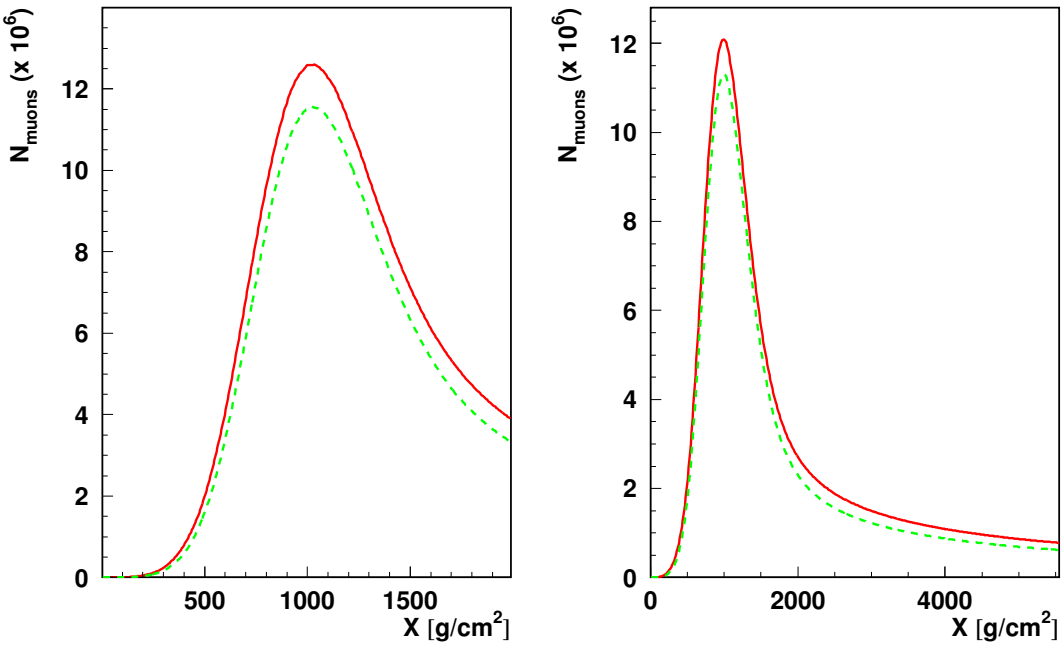

FIG. 5. Longitudinal development of muons for 10^{19} eV photon showers inclined 60 (left) and 80 (right) degrees. The solid (dashed) line corresponds to simulations with the present (old) model for photonuclear cross section.

For reasons of brevity, in this paper we present results only for the very representative case of 10^{19} eV gamma showers. At this primary energy, geomagnetic conversion [36] is not frequent, thus allowing photons to enter the atmosphere unconverted, and initiate normally the shower development. We have taken in most of our simulations a ground altitude of 1400 meters above sea level, corresponding to the altitude of current Cosmic Ray Observatories. In a few cases we have used for convenience a sea level ground altitude; this is explicitly indicated when it corresponds.

The most probable photon interactions at the mentioned energy are electromagnetic (i.e., pair production), and for that reason most of the shower secondaries will be electrons and photons; and the number of such secondaries is not expected to change substantially when replacing the photonuclear cross sections. This can clearly be seen in figure 4 where the average shower longitudinal development of electrons and positrons plotted show almost no differences between the old and present models.

On the other hand, muon production is noticeably increased when using the new photon cross sections. We present our results for the longitudinal development of muons in figure

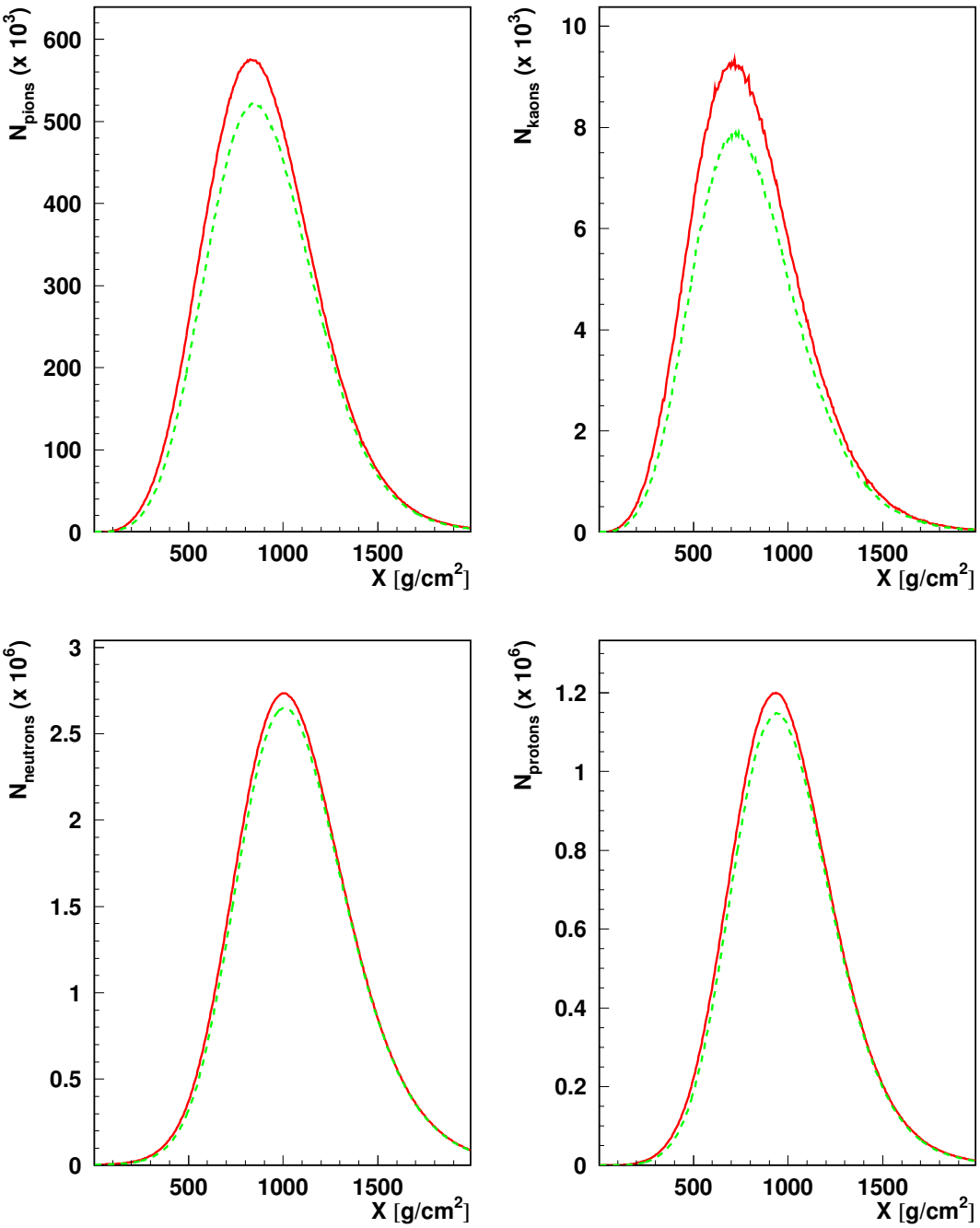

FIG. 6. Same as figure 4 but for the longitudinal development of hadrons: Upper left pions, upper right kaons, lower left neutrons, lower right protons.

5, where it is clearly seen that the simulations with the present model produce more muons in virtually the entire shower life. The relative difference with respect to the old model is about 12 % at the maximum ($X \simeq 1100$ g/cm^2). The difference persists even in the very late stage of shower development, as it can clearly be seen in the case of 80 degrees inclined

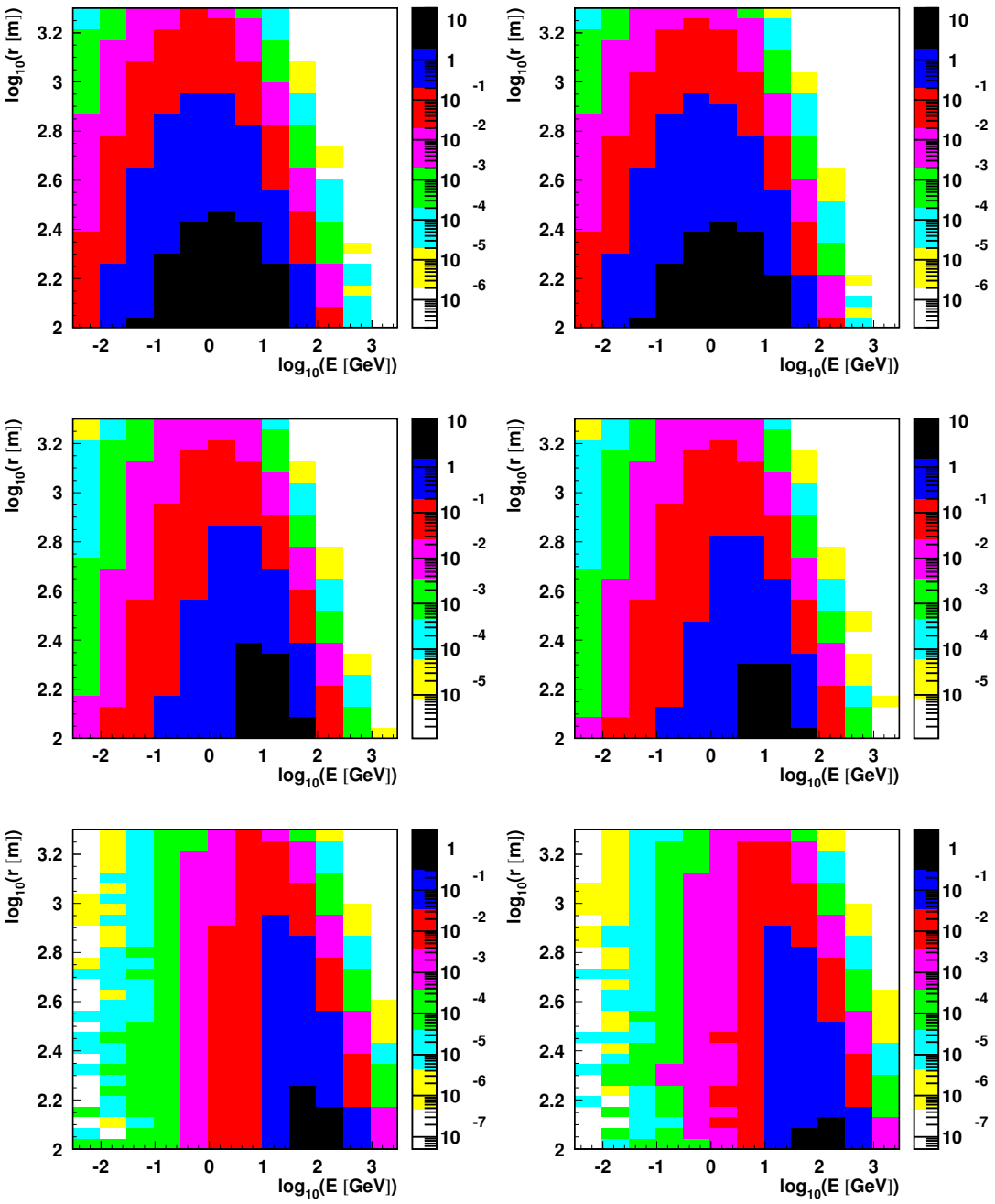

FIG. 7. Energy versus lateral (3d) distance to the shower axis distribution of ground muons for 10^{19} eV photon showers. The normalized density of muons $d\rho_\mu/d\log_{10} E$ (in m^{-2}) is represented in a color scale. The left (right) column plots correspond to simulations with the present (old) model for photonuclear cross sections. The upper, middle, and lower row plots correspond to zenith angles of 45, 60, and 80 deg respectively.

showers displayed at the right side of figure 5.

It is important to recall that shower muons are generated after the decay of unstable hadrons, mainly charged pions and kaons. Hence, the enlarged number of muons that shows up in figure 5 would be necessarily connected with enlarged hadron production, especially pions and kaons. The results of our simulations agree with this expectation. The results for the longitudinal development of charged pions, charged kaons, neutrons, and protons, plotted in figure 6 for the representative case of 10^{19} eV gamma showers inclined 60 degrees illustrate this point. These plots reveal a significant increase in the average number of produced pions and kaons, when comparing the simulations performed with the present model with the ones run with the old model. The plots for neutrons and protons also indicate noticeable but smaller increments. The current figures are obtained using QGSJET-II to simulate hadronic interactions. Simulations performed with other hadronic collision packages could give numerically different results, but with the characteristic that larger hadron production will always be expected in the case of the present mode because of its increased gamma-nucleus cross section, which enlarges the probability of hadronic collisions, especially for very energetic photons, present mostly at the early stages of shower development. The secondary particles generated after that initial shower multiplication process are the ones recorded in the plots of figure 6, and their number will be increased every time there is an increased hadronic collision probability.

It is also important to consider the characteristics of the muons produced in the simulations, especially those that reach the ground level. We will focus on the representative case of 10^{19} eV gamma showers with ground altitude 1400 m.a.s.l. This corresponds roughly to an atmospheric slant depth of 900 g/cm^2. Accordingly with the results displayed in figure 5, this depth is located short before the maximum of the muon longitudinal profile.

In figure 7 the two dimensional, energy versus 3d distance to the shower axis, normalized density distribution of ground muons is represented in a variety of cases. The left (right) column show the distributions obtained from simulations performed using the present (old) model for photonuclear cross sections. The upper, middle, and lower row plots correspond to shower inclinations with respect to the vertical of 45, 60, and 80 degrees, respectively. The color scales used to represent the muon densities are unique at each row. Comparing the distributions corresponding to the different inclinations it shows up clearly that the number of ground muons diminishes and their energy spectrum hardens as long as the zenith angle

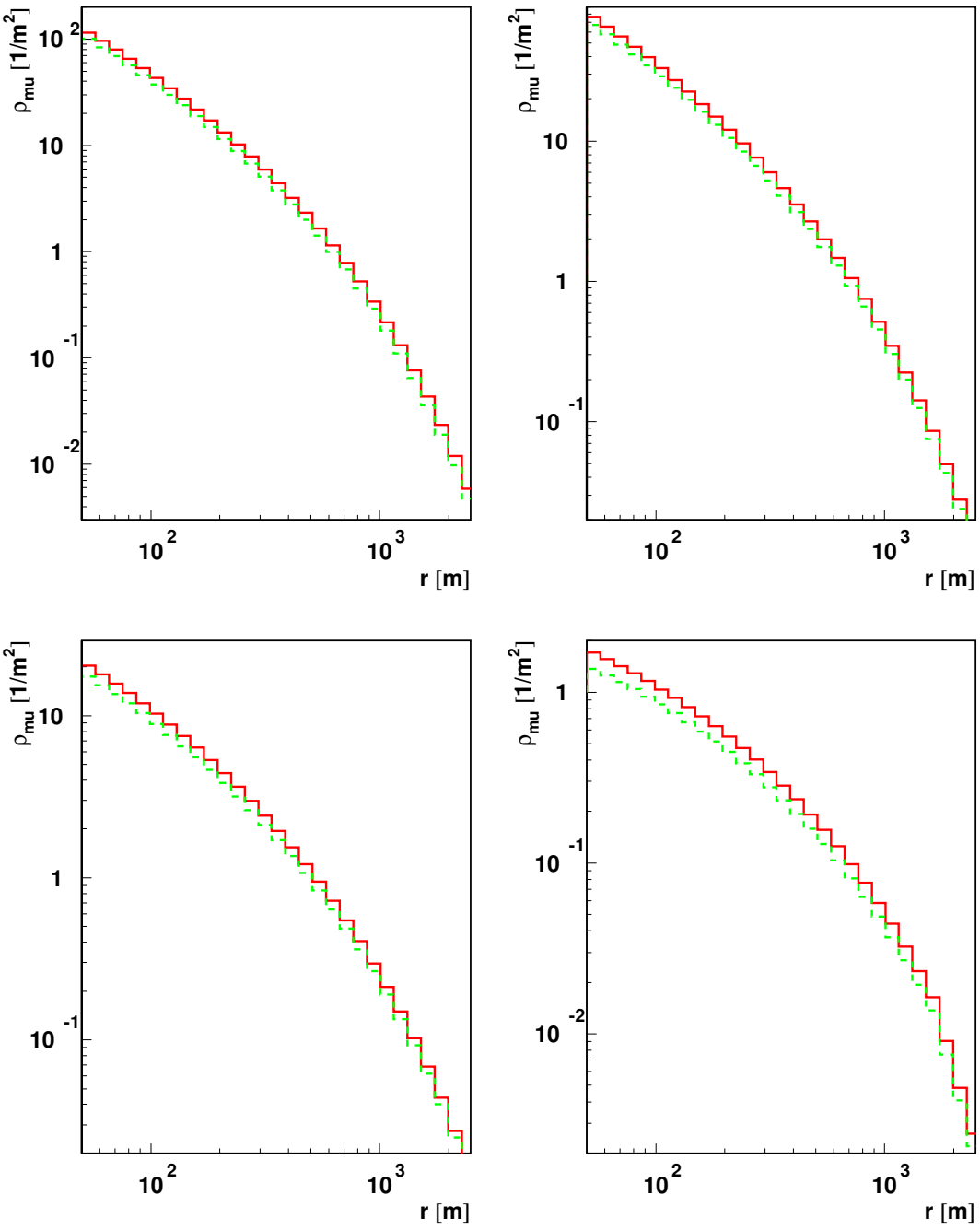

FIG. 8. Lateral distributions of ground muons for 10^{19} eV photon showers inclined 0 (upper-left), 45 (upper-right), 60 (lower-left), and 80 (lower-right) degrees. The solid (dashed) line corresponds to simulations with the present (old) model for photonuclear cross sections.

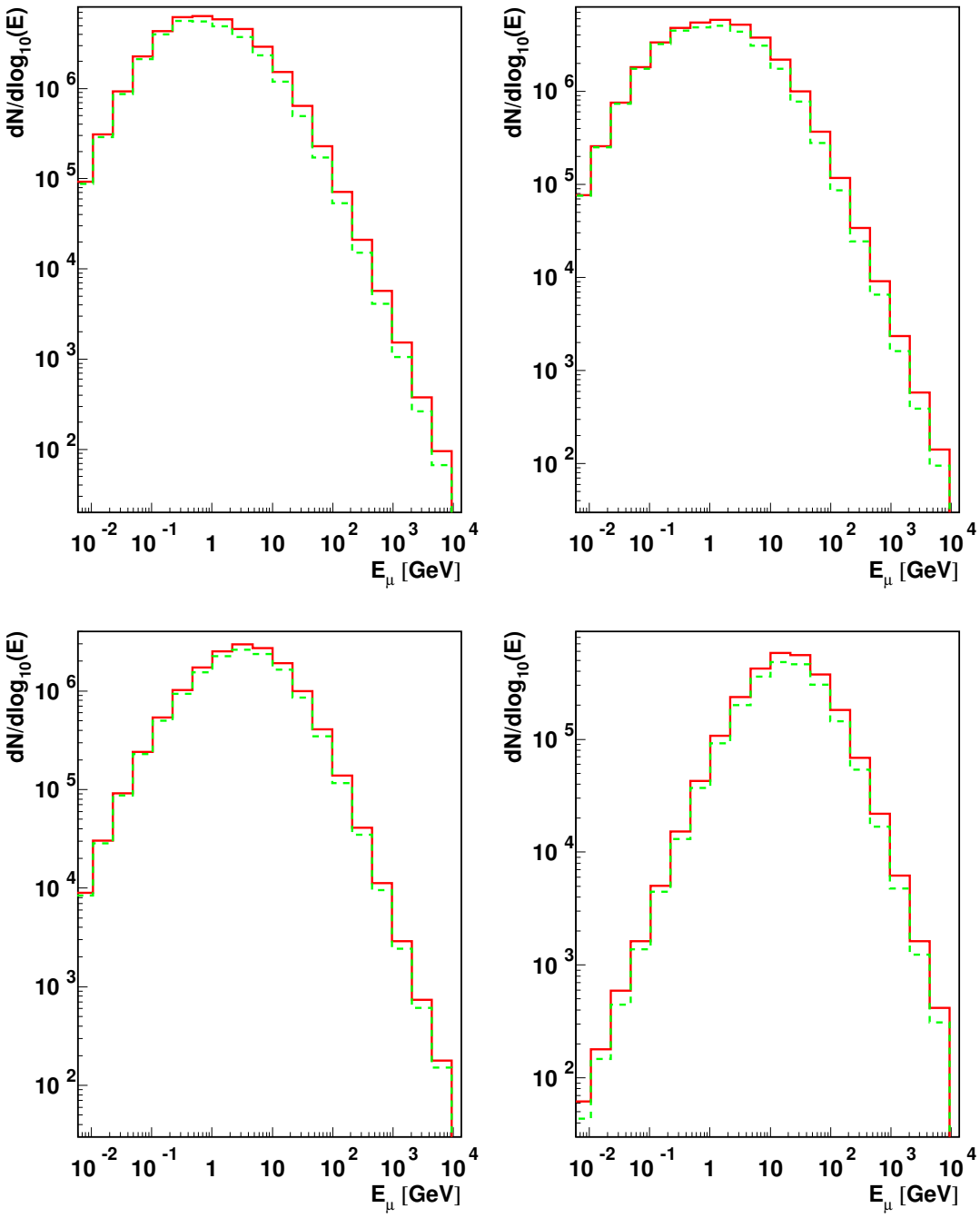

FIG. 9. Energy distributions of ground muons for 10^{19} eV photon showers inclined 0 (upper-left), 45 (upper-right), 60 (lower-left), and 80 (lower-right) degrees. The solid (dashed) line corresponds to simulations with the present (old) model for photonuclear cross sections.

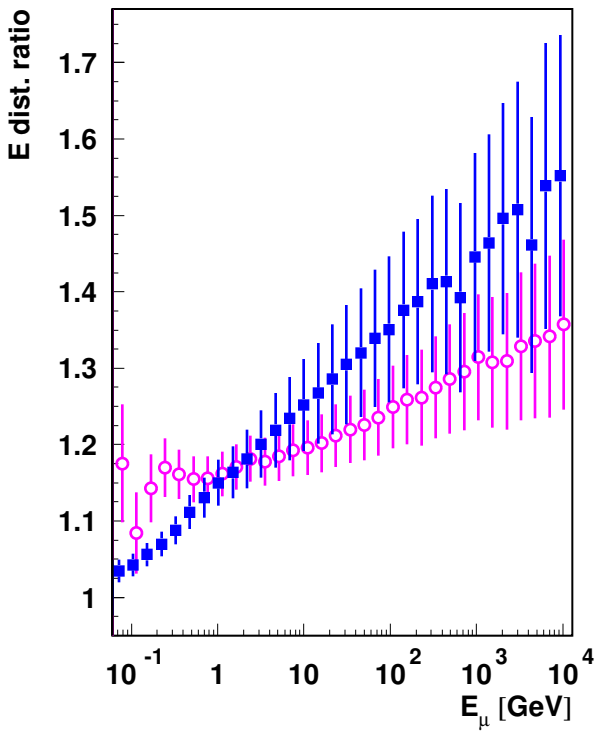

FIG. 10. Ratio between ground muon energy distributions obtained with the present and old models, for 10^{19} eV photon showers. The solid squares (open circles) correspond to a shower inclination of 45 (80) deg. Error bars are calculated by propagation of the individual RMS statistical errors of each of the distributions. The abscissas of the 80 deg data set have been shifted by 10% to improve error bar visibility.

is increased (notice the different color scales used at each angle). Needless to say, this is the expected behavior for showers of varying inclination, which at the same time will experiment a very significant change in the ratio between the electromagnetic and muon ground particle distribution (see for example reference [37]). When comparing the results corresponding to simulations performed using the present and old models of photonuclear cross sections (left and right column plots of figure 7, respectively), it is possible to notice that the densities of muons corresponding to the present model are larger than the respective ones for the old model. The differences are approximately independent of muon energy and distance to the shower axis, as will be discussed in more detail in the following paragraphs.

The lateral and energy distribution of ground muons for various shower inclination angles are displayed in figures 8 and 9, respectively. As in the case of the distributions in figure 7,

the simulations correspond to 10^{19} eV gamma showers, with ground altitude of 1400 m.a.s.l.

In the case of the lateral distribution of muons (figure 8), we observe that the distributions for the old and new photonuclear models are very similar in shape, differing only in the total number of particles. It can also be observed that the difference between photonuclear models becomes more significant for large zenith angles.

On the other hand, the muon energy distributions displayed in figure 9 present noticeable differences for muon energies greater than roughly 1 GeV, with the present model giving the largests number of particles at each bin. For muon energies lower than 1 GeV and zenith angles up to 60 degrees both distributions are virtually coincident; in the case of showers inclined 80 degrees the present model gives a larger number of particles in the entire muon spectrum. To better illustrate this characteristic of the impact of the photonuclear cross section on the average number of muons at ground, we also include plots of the ratio between both muon energy distributions. In figure 10, such ratios are plotted as functions of the muon energy for the representative cases of 45 (solid squares) and 80 (open circles) degrees of inclination. The increased number of high energy muons resulting after the simulations using the present model for photonuclear cross sections shows up clearly in the case of showers inclined 45 degrees, reaching average values of more than 50 % for muon energies of 10^4 GeV. In the case of showers inclined 80 degrees, the relative difference is always below 35 %, and remains virtually constant at 15 % approximately for muon energies below 1 GeV.

IV. FINAL REMARKS

The main objective of this paper is to present a QCD-based model for photoproduction, updated from the previous analysis [6] in light of recent LHC results for total pp cross sections, and to study the impact of this new model on the photon initiated air shower development. This model produces a photon-air nucleus total cross section significantly larger than the previous model included in the standard extended air shower studies. The present analysis based on simulations using the AIRES system clearly shows that for photon initiated showers the total muon production is increased in a measurable way. This result could be of direct importance in future determinations of bounds for the highest energy cosmic photon flux, particularly in the case of very inclined showers whose analysis is strongly based on ground muon distributions [38]. In this respect, a more detailed analysis of this

kind of effects is in progress.

ACKNOWLEDGMENTS

This collaboration was partially financed by the Programa de Cooperación Científico Tecnológico Argentino-Español: MinCyT-MINCINN AIC10-D-607. F.C. and A.G. acknowledge financial support from Junta de Andalucía (FQM-330, FQM-101, FQM-437, FQM6552) and MINECO FPA2013-47836-C3-1-P and Consolider-Ingenio 2010 program CPAN (CSD2007-00042). Partial support by CONICET and ANPCyT, Argentina, is also acknowledged.

[1] See *www.auger.org.*

[2] The Pierre Auger Collaboration, *Phys. Rev.,* **D90**, 122006 (2014).

[3] The Pierre Auger Collaboration, *Astroparticle Physics,* **31**, 399406 (2009).

[4] G. Antchev, et al., *Europhys. Lett.,* **101**, 21004 (2013).

[5] G. Antchev, et al., *Phys. Rev. Lett.,* **111 (1)**, 012001 (2013).

[6] R. M. Godbole, A. Grau, G. Pancheri and Y. N. Srivastava, *Eur. Phys. J.,* **C63**, 69-85 (2009)

[7] S. J. Sciutto, *Proc. 27th ICRC (Hamburg),* **1**, 237 (2001);
see also *www2.fisica.unlp.edu.ar/aires.*

[8] A. Corsetti, A. Grau, G. Pancheri and Y. N. Srivastava, *Phys. Lett,* **B382**, 282 (1996); A. Grau, G.Pancheri, Y. N. Srivastava, *Phys. Rev.,* **D60**, 114020 (1999); R. M. Godbole, A. Grau, G. Pancheri and Y. N. Srivastava, *Phys. Rev.,* **D72**, 076001 (2005).

[9] F. Bloch and A. Nordsieck, *Phys.Rev.,* **52**, 54 (1937).

[10] D. Cline, F. Halzen and J. Luthe, *Phys. Rev. Lett.,* **31**, 491 (1973).

[11] R. Biancastelli, C. Bosio, G. Matthiae , J. V. Allaby, W. Bartel, G. Cocconi, A. N. Diddens, R. W. Dobinson, A. M. Wetherell, *Phys. Lett.,* **B44**, 113 (1973).

[12] G. B. Yodh, Y. Pal and J. S. Trefil, *Phys. Rev. Lett.,* **28**, 1005 (1972).

[13] T. K. Gaisser and T. Stanev, *Phys. Lett.,* **B219**, 375 (1989).

[14] L. Durand and H. Pi, *Phys. Rev.,* **D40**, 1436 (1989).

[15] M. Froissart, *Phys. Rev.,* **123**, 1053-1057 (1961).

[16] M. Gluck, E. Reya, and A. Vogt, *Z. Phys.,* **C53**, 127–134 (1992); *Z. Phys.,* **C67**, 443–448 (1995); *Eur. Phys. J.,* **C5**, 461–470 (1998).

[17] A. D. Martin, R. G. Roberts, W. J. Stirling, and R. S. Thorne, *Phys. Lett.,* **B531**, 216–224 (2002).

[18] H.L. Lai, J. Botts, J. Huston, J. G. Morfin, J. F. Owens, Jian-wei Qiu, W. K. Tung, H. Weerts, *Phys. Rev.,* **D51**, 4763–4782 (1995).

[19] M. Glück, E. Reya and A. Vogt, *Phys. Rev.,* **D46**, 1973 (1992).

[20] M. Glück, E. Reya and I. Schienbein, *Phys. Rev.,* **D60**, 054019 (1999); Erratum, *ibid,* **D62**, 019902 (2000).

[21] F. Cornet, P. Jankowski, M. Krawczyk and A. Lorca, *Phys. Rev.,* **D68**, 014010 (2003).

[22] A. Corsetti, A. Grau, G. Pancheri and Y.N. Srivastava, *Phys. Lett.,* **B382**, 282-288 (1996).

[23] M. Greco and P.Chiappetta, *Nucl. Phys.,* **B221**, 269 (1983).

[24] D.A. Fagundes, A. Grau, G. Pancheri, Y.N. Srivastava and O. Shekhovtsova, *Phys. Rev.,* **D91**, 114011 (2015).

[25] A. Grau, R. M. Godbole , G. Pancheri, Y. N. Srivastava, *Phys. Lett.,* **B682**, 55-60 (2009).

[26] A. Achilli, R. M. Godbole, A. Grau, R. Hegde, G. Pancheri and Y. Srivastava, *Phys. Lett. B,* **659**, 137 (2008).

[27] The Pierre Auger Collaboration, *Phys. Rev. Lett.,* **109**, 062002 (2012).

[28] R. S. Fletcher, T. K. Gaisser and F. Halzen, *Phys. Lett.,* **B298**, 442 (1993); *Phys. Rev.,* **D45**, 377–381 (1992), Erratum, *ibid,* **D45**, 3279 (1992).

[29] J. C. Collins and G. A. Ladinsky, *Phys. Rev.,* **D43**, 2847 (1991).

[30] G. Aad *et al.* (ATLAS Collaboration), *Nucl. Phys.,* **B889**, 486 (2014).

[31] M. M. Block and F. Halzen, *Phys.Rev.,* **D70**, 091901 (2004).

[32] M. M. Block, L. Durand and P. Ha, *Phys. Rev.,* **D89**, 094027 (2014).

[33] A. Martin, W. Stirling, R. Thorne and G. Watt, *Eur. Phys. J.,* **C 63**, 189 (2009).

[34] S. Ostapchenko, *Nucl. Phys. Proc. Suppl.,* **B151**, 143 (2006).

[35] K.A. Olive et al. (Particle Data Group), *Chin. Phys. C,* **38**, 090001 (2014); see also *pdg.lbl.gov.*

[36] P. Billoir *et al.,* for The Pierre Auger Collaboration, *Proc. 27th ICRC (Hamburg),* **1**, 718 (2001).

[37] A. Cillis, S. J. Sciutto, *J. Phys. G,* **26**, 309 (2000).

[38] The Pierre Auger Collaboration, *Phys. Rev.,* **D91**, 032003 (2015).